

Introduction

Reverse time migration (RTM) is now a well-established tool for pre-stack imaging in complex geological area, driven by the increase in capacity of computation. Considering combination of PP and PS images can characterize the reservoir more accurately (Stewart et al., 2002). The elastic RTM (ERTM) has been a promising imaging method for achieving more accurate and physical-related imaging result than acoustic RTM for both isotropic and anisotropic media.

From the beginning of the study on ERTM (Chang and McMechan, 1987), it has been discussed and extended on various aspects, e.g. imaging condition (Yan and Sava, 2007; Chung et al., 2012; Ravasi and Curtis, 2013b) and angle gather generation (Yan and Xie, 2010; McGarry and Qin, 2013; Wang et al., 2014). RTM applies imaging condition to the forward (source) and the backward (receiver) wavefields which are both extrapolated by solving a two-way wave equation (Baysal et al., 1983; McMechan, 1983). In isotropic media, a pure P- or S-wave source can be easily implemented by disturbing the stress components. However, the same operation will generate source wavefields with both P- and S-wave components in anisotropic media. To produce physically interpretable images using ERTM, mode decoupling before the application of the imaging condition is required to avoid artifacts from crosstalk of P- and S-wave modes (Yan and Sava, 2007). Considering elastic anisotropy, Wang et al. (2014) suggested to separate the wave modes in both source and receiver wavefields before applying imaging condition for angle gather extraction. In practice, we have only a smooth velocity model at hand. So the S-wave components are mainly generated by the source instead of mode conversion during wavefield extrapolation. To avoid expensive mode separation during forward wavefield extrapolation, we propose an approach to numerically simulate a pure wave source in anisotropic media. It can be used for ERTM and waveform inversion of multi-component seismic data from active source (surface or borehole) and passive source (microseismic or earthquake). For applying it to ERTM of surface seismic data, we use tensorial wavefield extrapolation to mitigate nonphysical waves resulting from reverse-time “injection” of the particle displacements (or velocities) recorded at the receiver locations (Ravasi and Curtis, 2013a).

Methodology

From the physical point of view, a pure wave source can be numerically simulated by adding a disturbance on the component of vector wavefields to yield the polarization pattern of the given wave mode in the real media. Isotropic P-wave polarizes in the direction of the wave vector, $\mathbf{k} = (k_x, k_y, k_z)$, which is independent of medium parameters. This ensures that an isotropic P wave source can be easily implemented. In anisotropic media, the qP or qS-wave mode generally has its own polarization vector not parallel or perpendicular to the wave vector. We name a source that generates only pure-mode wavefields as an intrinsic pure wave source. However, the intrinsic pure wave source is almost impossible for operation in field work and seldom observed in earthquake or microseismic events.

We propose an approach to obtain a numerical qP-wave source at the beginning of forward extrapolation from the actual source wavefields (generally containing qS-wave energy) in anisotropic media. This numerical source preserves the kinematic and dynamic characteristics of qP-wave resulting from the actual source and is free of qS-wave contamination. To realize this, we need to review the approach of vector decomposition for elastic wavefields (Zhang and McMechan, 2010).

In isotropic media, a vector wavefields $\mathbf{U} = \{U_x, U_y, U_z\}$ can be decomposed into a curl-free P-wavefields and a divergence-free S-wavefields: $\mathbf{U} = \mathbf{U}^P + \mathbf{U}^S$. In Fourier domain, vector P-wave fields can be decomposed from the total wavefield using

$$\widetilde{u}_i^P(\mathbf{k}) = \bar{k}_i \cdot \bar{k}_j \cdot \widetilde{u}_j(\mathbf{k}), \quad (1)$$

where \widetilde{u}_i is the component of original elastic wavefields in wavenumber domain and \bar{k}_i represents the component of the normalized wave vector $\bar{\mathbf{k}}$. The summation convention is used in this abstract. In TI medium, equation (1) can be extended as:

$$\widetilde{u}_i^{qP}(\mathbf{k}) = \bar{\mathcal{P}}_i(\mathbf{k}) \cdot \bar{\mathcal{P}}_j(\mathbf{k}) \cdot \widetilde{u}_j(\mathbf{k}), \quad (2)$$

in which $\bar{\mathcal{P}}_i(\mathbf{k})$ stands for the normalized polarization component of qP-wave. In general the normalized polarization vectors can be determined by solving the Christoffel equation.

In field work, people often excite a source with coupled qP- and qS-wave modes if the medium at the source location shows elastic anisotropy. According to the vector decomposition equation, we can obtain a numerical qP-wave source using

$$\mathcal{S}_i^{qP}(\mathbf{x}) = \int e^{i\mathbf{k}\cdot\mathbf{x}} \bar{\mathcal{P}}_i(\mathbf{x}, \mathbf{k}) \cdot \bar{\mathcal{P}}_j(\mathbf{x}, \mathbf{k}) \cdot \tilde{G}(\mathbf{k}) d\mathbf{k}, \quad (3)$$

where $\mathcal{S}_i^{qP}(\mathbf{x})$ is the component of qP-wave source, G represents the dyadic Green's function that satisfies the elastic wave equation for a actual source term (e.g., an explosive source, a strike-slip source, etc.). Note that the Green's function can be calculated within a small region around the source location at the beginning of forward wavefield extrapolation.

To apply the numerical pure wave source to ERTM for anisotropic media, we forward extrapolate the source wavefields using the numerical qP-wave source simulated with equation 3. The receiver wavefields is reverse-time extrapolated and separated into qP- and qS-wave modes using the fast algorithm proposed by Cheng and Fomel (2014). In fact, injection of particle displacement or velocity data as boundary condition may result in artifacts in the extrapolated receiver wavefields due to the following two issues: First, the injected energy will upward and downward propagate simultaneously; Second, every event will emit P- and S-wave modes. Ravasi and Curtis (2013a) suggested to combine the stress and particle velocity data as the new boundary condition with a background velocity (Equation 7 in their paper). This approach is designed for general elastic wave propagation. We apply it to ERTM with the help of numerical qP-wave source implementation and efficient wave mode separation for anisotropic media.

Numerical example

Figure 1 shows the snapshots of wavefields from an explosive source (equivalent forces on normal stress components) and the numerical qP-wave source in a VTI media. Obviously the explosive source excites qS-wave energy in anisotropic media, but the numerical qP-wave source only excites pure-mode qP-wave fields. The spatial pattern of the numerical qP-wave source (Figure 1b and 1e) is material-dependent in anisotropic media as previously discussed. To show the advantage of implementing pure wave source in ERTM with tensorial wavefields extrapolation, we use a VTI medium as constant background and with a single point scatterer, $\Delta\rho = 600\text{kg}/\text{m}^3$, at the location of $\mathbf{x}_{scatter}(1000, 600)\text{m}$. The source is triggered at $\mathbf{x}_s(1400, 50)\text{m}$, and all the receivers are put at 300 m below the surface. Ravasi and Curtis (2013a) had used a similar model for an isotropic ERTM issue. Regarding anisotropy, we use the fast algorithm of mode separation (Cheng and Fomel, 2014) to obtain the scalar qP- or qSV-wave fields. In the first row of Figure 2, the same explosive source is used to synthesize the data and simulate the source wavefields for ERTM. We observe two more events caused by the qS-wave (a weak SP and a strong SS) energy in the backward extrapolated (scalar) qP- or qSV-wave fields. The PP and PS ERTM images for the data of explosive source (Figure 2b and 2c) show two types of artifacts, in which, one is resulted from the SP or SS event in the backward extrapolated wavefields (red arrows), and the other is from the qS-wave energy excited by the source in the forward extrapolated wavefields (white arrow). The bottom row of Figure 2 show the corresponding backward extrapolated (scalar) qP-wave fields and the ERTM images when the numerical pure qP-wave source is used. We obtain extrapolated wavefields without qS-wave artifacts at the receiver side (as well as the source side, but not shown here) and more clean ERTM results for both PP and PS data.

Conclusions

we propose a general approach to numerically simulate the pure wave source for elastic wave propagation. It may be useful for seismic imaging and waveform inversion when the real source is located in an anisotropic media. Combining pure P wave source with fast wave mode separator, we extend the tensorial wavefield extrapolation into anisotropic media in synthetic example.

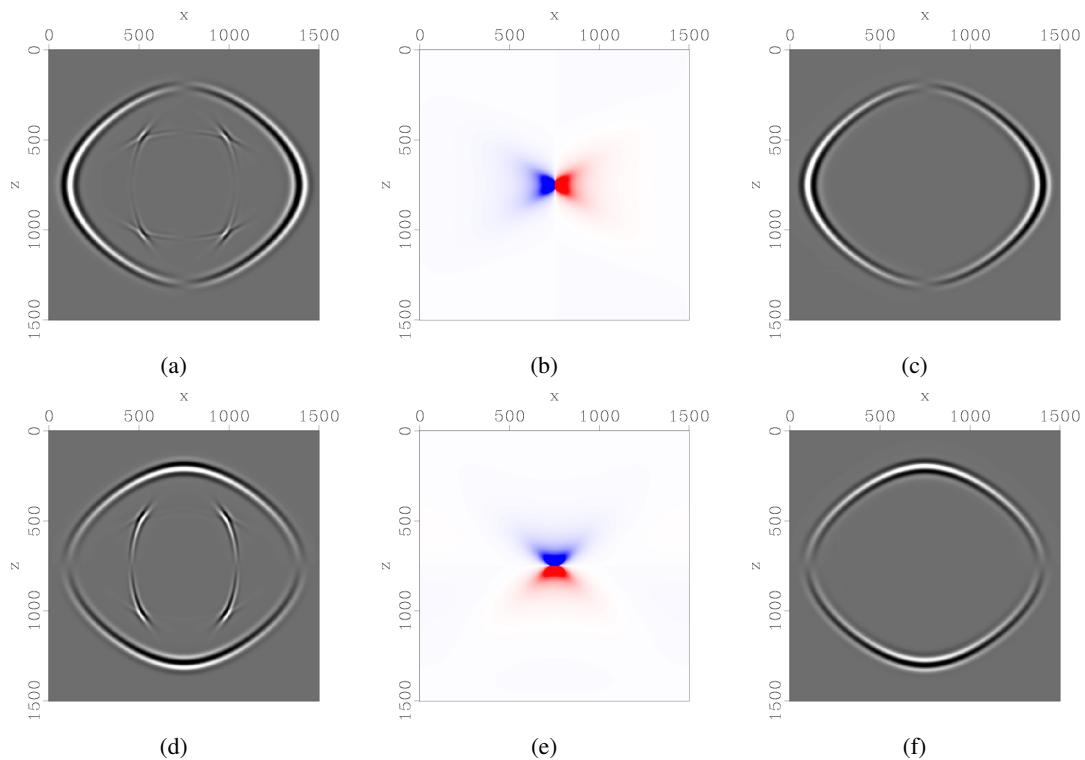


Figure 1: Vector wavefield snapshots in a VTI medium ($v_{p0} = 2600m/s, v_{s0} = 1400m/s, \epsilon = 0.2, \delta = -0.1$) using staggered-grid finite difference algorithm: (a)x- and (d) z-component of particle velocity fields using an explosive source; (b)x- and (e) z-component of the source pattern of the numerical pure qP-wave source; (c)x- and (f) z-component of particle velocity fields using the pure qP-wave source.

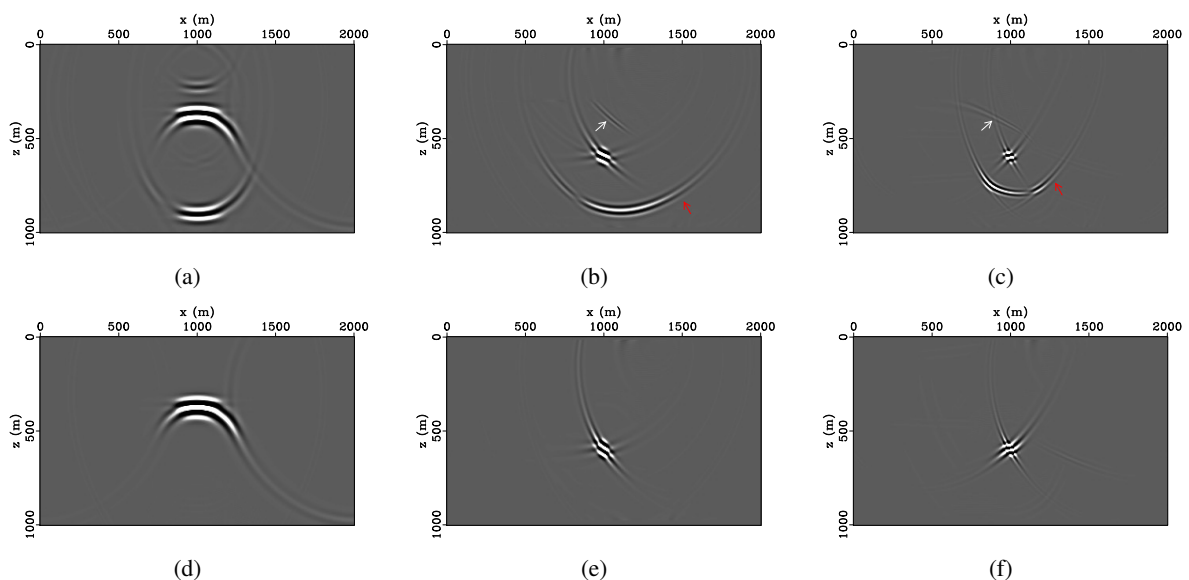


Figure 2: Backward extrapolated wavefields and ERTM images of a scattering point using an explosive source (top) and a numerical pure qP-wave source (bottom) in a VTI medium ($v_{p0} = 2600m/s, v_{s0} = 1400m/s, \epsilon = 0.2, \delta = 0.1$): (a) and (d) are backward extrapolated (scalar) qP-wave fields at the time of 0.4s; (b) and (e) are PP image of single shot ERTM; (c) and (f) are PS image of single shot ERTM;

Acknowledgement

This work was supported by China Scholarship Council (NO.201406260132) and the National Natural Science Foundation of China (NO.41474099). C.L. Wang would like to thank M. Ravasi, Q. Hao and W. Weibull for interesting and helpful discussions. We appreciate the ROSE consortium for providing the computation and working environment and acknowledge the support of Madagascar open-source package freely from: <http://www.reproducibility.org>.

REFERENCES

- Baysal, E., D. D. Kosloff, and J. W. Sherwood, 1983, Reverse time migration: *Geophysics*, **48**, 1514–1524.
- Chang, W.-F., and G. A. McMechan, 1987, Elastic reverse-time migration: *Geophysics*, **52**, 1365–1375.
- Cheng, J., and S. Fomel, 2014, Fast algorithms for elastic-wave-mode separation and vector decomposition using low-rank approximation for anisotropic media: *Geophysics*, **79**, C97–C110.
- Chung, W., S. Pyun, H. S. Bae, C. Shin, and K. J. Marfurt, 2012, Implementation of elastic reversetime migration using wavefield separation in the frequency domain: *Geophysical Journal International*, **189**, 1611–1625.
- McGarry, R., and Y. Qin, 2013, Direction-vector-based angle gathers from anisotropic elastic rtm: SEG Technical Program Expanded Abstracts, 3820–3824.
- McMechan, G., 1983, Migration by extrapolation of time-dependent boundary values: *Geophysical Prospecting*, **31**, 413–420.
- Ravasi, M., and A. Curtis, 2013a, Elastic imaging with exact wavefield extrapolation for application to ocean-bottom 4c seismic data: *Geophysics*, **78**, S265–S284.
- , 2013b, Nonlinear scattering based imaging in elastic media: Theory, theorems, and imaging conditions: *Geophysics*, **78**, S137–S155.
- Stewart, R., J. Gaiser, R. Brown, and D. Lawton, 2002, Convertedwave seismic exploration: Methods: *Geophysics*, **67**, 1348–1363.
- Wang, C., J. Cheng, and T. Wang, 2014, Angle domain elastic reverse time migration in ti media: EAGE Extended Abstracts, G103.
- Yan, J., and P. Sava, 2007, Elastic wavefield imaging with scalar and vector potentials: SEG Technical Program Expanded Abstracts, 3820–3824.
- Yan, R., and X.-B. Xie, 2010, The new angle-domain imaging condition for elastic rtm: SEG Technical Program Expanded Abstracts, 3820–3824.
- Zhang, Q., and G. A. McMechan, 2010, 2d and 3d elastic wavefield vector decomposition in the wavenumber domain for vti media: *Geophysics*, **75**, D13–D26.